Biochimica et Biophysica Acta 932 (1988) 287–305
Elsevier

BBA 42714

Theory for spectral hole burning of the primary electron donor state of photosynthetic reaction centers

J.M. Hayes, J.K. Gillie, D. Tang and G.J. Small

Ames Laboratory-USDOE and Department of Chemistry, Iowa State University, Ames, IA (U.S.A.)

(Received 27 July 1987)

Key words: Hole burning spectroscopy; Electron phonon coupling; Photosynthesis; Reaction center

A theory for solid state spectral hole burning is developed. The theory is valid for arbitrarily strong linear electron-phonon coupling within the Condon approximation which is accurate for strongly allowed optical transitions. Model calculations show that, from the dependence of the hole profile on the burn frequency, the contribution to the absorption linewidth from site inhomogeneity and the linear coupling parameters can be determined. The theory is used to analyze recent hole-burning data on the primary electron-donor states of isolated reaction centers of *Rhodopseudomonas viridis*, *Rhodobacter sphaeroides* and Photosystem I. The results show that all of these states are characterized by strong linear electron-phonon coupling (Huang-Rhys factor $S \gtrsim 4$) and large site inhomogeneous line broadening.

Introduction

In attempts to understand electronic excitation transport and electron transfer in photosynthetic units a variety of spectroscopic techniques have been utilized. Most recently, frequency domain spectral hole burning [1–7], which complements ultra-fast time-domain techniques, has been applied to the primary electron donor state of photosystem I [8,9] and the bacterial systems *Rhodobacter sphaeroides* [10,11] and *Rhodopseudomonas viridis* [12,13]. In addition, hole burning has been reported for a core antenna complex (C-670) of PS I [14]. Irrespective of whether the hole-burning mechanism is photochemical [5] (as is the case for the primary electron donor state) or nonphotochemical [4,7] (as appears to be the case for the core antenna complex C-670 of Photosystem I [14]), the data relate to several important questions. Included are the intramolecular vibronic activity in the pigment absorption, pigment site inhomogeneity within the protein complex, electronic excitation transport and electron transfer dynamics and the electron-phonon coupling. By phonon is meant low-frequency ($\lesssim 100$ cm^{-1}, or $\lesssim 3 \cdot 10^{12}$ Hz) modes of the pigment-protein complex.

The role of the electron-phonon coupling in nonadiabatic electronic excitation transport from the antenna to the primary electron donor state of the reaction center and electron transfer within the reaction center poses an interesting question. From the point of view of dynamics, one is asking about the function of the protein beyond that of a glue which defines the relative orientations of the photosynthetic pigments. Phonons (approx. 100 cm^{-1}) have recently been implicated as the key

Abbreviations: B800 and B835, bacteriochlorophyll absorptions at 800 and 835 nm; C-670, core antenna complex of Photosystem I absorbing at 670 nm; PS I, Photosystem I; P-700, P-870 and P-960, the primary electron donors of Photosystem I, *Rhodobacter sphaeroides* and *Rhodopseudomonas viridis*, respectively; PVOH, poly(vinyl alcohol).

Correspondence: G.J. Small, Ames Laboratory-USDOE and Department of Chemistry, Iowa State University, Ames, IA 50011, U.S.A.

modes for nuclear tunneling associated with the quinone reduction and its subsequent charge recombination in the reaction center of *Rb. sphaeroides* [15,16]. Hole-burning studies on C-670 and the primary electron donor state P-700 of PS I have led to the conclusion that low frequency (approx. 30 cm^{-1}) phonons are the primary acceptor modes for nonadiabatic electronic excitation transport from the antenna to P-700 [14]. At the same time, theoretical analysis of hole-burning data for P-700 [14] and P-870 [17] showed that these primary electron donor states are characterized by strong electron-phonon coupling. The possibility exists, therefore, that low-frequency phonons are of fundamental importance for transport phenomena in the photosynthetic unit. The nature of these phonons remains an open question.

The primary purpose of this paper is to present a unified picture for the linear electron-phonon coupling associated with the primary electron donor states P-700, P-870 and P-960 of PS I, *Rb. sphaeroides* and *Rps. viridis*. To this end, the details of the theory for hole burning in the presence of arbitrarily strong linear electron-phonon coupling are presented along with refined calculations of the hole spectra for the above three states. A brief discussion of the theory has been given in Ref. 17 where it was applied to the data of Boxer and coworkers [10] on P-870. Exceedingly broad holes (approx. 400 cm^{-1}) were observed at 1.5 K for several burn frequencies (ω_B) located within the P-870 absorption profile. The maximum of the hole did not generally coincide with ω_B and its position was not invariant to variations in ω_B. Furthermore, the holewidth was observed to increase with increasing ω_B. Time-domain studies had earlier shown that electron transfer from the special pair (P-870) to the bacteriopheophytin of the reaction center takes place in about 2 ps at cryogenic temperatures [16]. The width of a zero-phonon hole corresponding to this transfer time is approx. 2.5 cm^{-1}. Thus, the absence of a sharp hole for P-870 was particularly interesting [10]. The hole-burning properties of P-870 were shown to be consistent with (i) strong linear electron-phonon coupling defined by a Huang-Rhys factor $S \approx 8$ and a mean phonon frequency $\omega_m \approx 30\ cm^{-1}$ and (ii) a site inhomogeneous absorption linewidth contribution of $\Gamma_{inh} \approx 400\ cm^{-1}$ [17]. The S and ω_m values were chosen to be consistent with the analysis by Scherer et al. [18] of absorption and fluorescence thermal broadening and Stokes shift (approx. $2S\omega_m$) data for P-960. The thermal broadening data were a compilation of results from several different laboratories. Data are presented here that are far more precise and used to refine the hole-burning calculations for P-870.

These thermal broadening data together with the same for P-960 are also used to conclude that Γ_{inh} for P-870 is approx. 200 cm^{-1} greater than for P-960. As a result, the hole-burning characteristics for P-960 [12] can be understood with one and the same model which accounts for the data for P-870. The key difference between the data is that the broad hole maximum frequency for P-960 is insensitive to variations in ω_B [12].

Gillie et al. [9] have shown that the hole profiles for P-700 of enriched PS I particles from spinach consist of a very weak but sharp zero-phonon hole (coincident with ω_B) superimposed on an intense but broad hole whose width is comparable to those observed for P-870 and P-960. Maslov et al. [8] had earlier observed the sharp feature for P-700 of intact cells of a mutant strain of *Chlamydomonas reinhardtii*. The data of Ref. 9 were also shown to be consistent with strong linear electron-phonon coupling plus significant site inhomogeneous line broadening. Refined calculations for P-700 presented here are discussed in terms of those for P-870 and P-960.

Theory

The single-site absorption profile

For the case of arbitrarily strong electron-phonon coupling it is convenient to determine the Fourier transform of the absorption lineshape function $G(\Omega)$ [19]:

$$g(t) = \int d\Omega\, G(\Omega)\, e^{i\Omega t} \tag{1}$$

where

$$G(\Omega) = \langle \sum_{n'} |\langle fn' | \underline{d} | on \rangle|^2 \delta(\Omega) - \{ E_{f,n'} - E_{o,n} \}/\hbar \rangle_T \tag{2}$$

and $\langle\ \rangle_T$ denotes a thermal average over initial

phonon levels n of the ground state. The subscripts f and n' denote the excited electronic state and its phonon levels, respectively and $\underset{\sim}{d}$ is the electric dipole moment operator. In the adiabatic approximation the transition dipole takes the form

$$\langle fn' | \underset{\sim}{d} | on \rangle = \underset{\sim}{M}_o \prod_\alpha \left\langle n'_\alpha | n_\alpha \right\rangle + \sum_\alpha \underset{\sim}{m}_\alpha \left\langle n'_\alpha | q_\alpha | n_\alpha \right\rangle \prod_{\beta \neq \alpha} \left\langle n'_\beta | n_\beta \right\rangle \tag{3}$$

where the first and second terms represent the Condon and phononic contributions, respectively. The phonon coordinates q_α are those of the ground state and the $\underset{\sim}{m}_\alpha$ are the induced electronic transition dipoles. The phonons are comprised of all intermolecular modes and provide a density of states, $\rho(\omega)$. We consider the case where the phonons are sufficiently delocalized so that for each and every q_α its displacement, a_α, in the excited electronic state is of order $N^{-1/2}$, where N is the number of molecular entities comprising the system. We discuss at the end the case where a pseudolocalized [20] phonon exists and undergoes a large displacement. The displacement a_α is defined by expressing the excited-state potential as

$$E_f(\underset{\sim}{q}) = E_f(o) + \sum_\alpha A_\alpha q_\alpha + \tfrac{1}{2} \sum_{\alpha,\beta} B_{\alpha\beta} q_\alpha q_\beta \tag{4}$$

in the harmonic approximation. The second term represents the linear electron-phonon coupling. For our application the phonon normal coordinate rotation can be ignored, i.e., $B_{\alpha\beta} = \omega'^2_\alpha \delta_{\alpha\beta}$ and, further, we take $\omega'_\alpha = \omega_\alpha$ (ground state frequency). Eqn. 4 can be rewritten as

$$E_f(\underset{\sim}{Q}) = E_f(o') + \tfrac{1}{2} \sum_\alpha \omega_\alpha^2 Q_\alpha^2 \tag{5}$$

where the $Q_\alpha = q_\alpha + a_\alpha$ are the excited-state phonon coordinates and $a_\alpha = A_\alpha / \omega_\alpha^2$. The term

$$E_f(o') - E_f(o) = \tfrac{1}{2} \sum_\alpha (a_\alpha \omega_\alpha)^2 \tag{6}$$

represents the difference between the vertical and adiabatic absorption transition frequencies. And so for $\omega_\alpha = \omega'_\alpha$, the Stokes shift at $T = 0$ K (energy difference between the intensity maxima in absorption and fluorescence) is

$$\text{Stokes shift}(T = 0\ \text{K}) = \sum_\alpha (a_\alpha \omega_\alpha)^2 \tag{7}$$

We consider this shift for finite temperatures later.

For the case of delocalized phonons and $|\underline{m}_\alpha| \approx N^{-1/2} |\underline{M}_o|$ the right-hand side of Eqn. 3 is readily evaluated perturbatively. The procedure involves using the ground-state phonon wavefunctions as a zero-order basis set with the perturbation $\sum_\alpha A_\alpha Q_\alpha$ to determine the excited-state phonon wavefunctions. We will, however, consider here only the Condon contribution, since our application is to a strongly allowed electronic transition, i.e., $|m_\alpha| \ll N^{-1/2} |M_o|$. It follows that

$$g(t) = e^{i\nu t} \prod_\alpha \left\{ 1 - \tfrac{1}{2} (\gamma_\alpha^{1/2} a_\alpha)^2 [(2\langle n_\alpha \rangle_T + 1)(1 - \cos \omega_\alpha t) - i \sin \omega_\alpha t] \right\} \tag{8}$$

to order N^{-1}, where ν is the zero-phonon transition frequency, $\gamma_\alpha = \omega_\alpha / \hbar$ and $\langle n_\alpha \rangle_T$ is the phonon thermal occupation number equal to $[\exp(\hbar\omega_\alpha / kT^{-1})]^{-1}$. The product Π_α term can be expressed as

$$1 - \tfrac{1}{2} \sum_\alpha (\gamma_\alpha^{1/2} a_\alpha)^2 \left\{ \left(\coth \frac{\hbar \omega_\alpha}{2kT} \right) (1 - \cos \omega_\alpha t) - i \sin \omega_\alpha t \right\}$$

and the sum replaced by

$$\sum_\alpha \to h^{-1} \int_0^{\omega_M} d\omega\ \omega a_\omega^2 \rho(\omega)$$

where $\rho(\omega)$ is the phonon density of states and ω_M the maximum fundamental phonon frequency. Defining

$$A(\omega) = \tfrac{1}{2} \omega a_\omega^2 \rho(\omega) \tag{9}$$

it follows that

$$g(t) = e^{i\nu t} e^{-S(1 - \xi(t))} \tag{10}$$

Here S is the Huang-Rhys factor,

$$S = \sum_\alpha (\langle n_\alpha \rangle_T + \tfrac{1}{2}) (\gamma_\alpha^{1/2} a_\alpha)^2 = \int d\omega\ A(\omega) \coth \frac{\hbar \omega}{2kT} \tag{11}$$

and

$$\xi(t) = S^{-1}\int d\omega \left[\cos \omega t \coth\frac{\hbar\omega}{2kT} + i \sin \omega t\right] A(\omega) \qquad (12)$$

Eqn. 10 is exact to order N^{-1}. Now

$$G(\Omega) = \frac{1}{2\pi}\int dt\, g(t)\, e^{-i\Omega t} \qquad (13)$$

which with Eqn. 10 becomes

$$G(\Omega) = e^{-S}\sum_{r=0}^{\infty}\frac{S^r}{r!}B_r(\Omega) \qquad (14)$$

with

$$B_r(\Omega) = \frac{1}{2\pi}\int dt\, e^{i(\nu-\Omega)t}(\xi(t))^r \qquad (15)$$

The r values of 0, 1, 2, ... correspond to zero-, one-, two-, etc. phonon transitions in which no single phonon undergoes a quantum number change of greater than 1. Thus, $B_r(\Omega)$ is the line shape function for the r-phonon ($|n' - n| = r$) process and is normalized to unity as written. From Eqn. 15 the zero-phonon line is a delta-function centered at ν as expected because no allowance for dephasing has yet been made. It is also apparent that the r-phonon lineshape is the result of convolving $B_1(\Omega)$ r-times with itself, vide infra. With Eqns. 12 and 15 it follows that

$$B_1(\Omega) = S^{-1}\int d\omega\, A(\omega)\left(\frac{\delta(\nu-\Omega+\omega)}{1-e^{-\hbar\omega/kT}} + \frac{\delta(\nu-\Omega-\omega)}{e^{\hbar\omega/kT}-1}\right) \qquad (16)$$

where the first and second terms correspond to one-phonon creation and annihilation, respectively. Eqn. 16 serves to underscore the fact that $B_r(\Omega)$ takes due account of all phonon transitions for which $|\Sigma_\alpha(n'_\alpha - n_\alpha)| = r$ subject to the aforementioned constraint. Because $B_r(\Omega)$ is normalized to unity the weighting factor for the r-phonon process is

$$P_r = e^{-S}\frac{S^r}{r!} \qquad (17)$$

From Eqn. 16 it is evident that the function A determines, aside from the thermal factors, the shape of the one-phonon spectrum. In the $\lim_{T\to 0}$ only the first term survives and $A(\Omega - \nu)$ is completely determining. This function is difficult to calculate, cf. Eqn. 9, and so we turn to experiment as a guide. Fluorescence-line-narrowed spectra of impurities in organic glasses and polymers exhibiting weak electron-phonon coupling ($S < 1$) often exhibit a one-phonon line shape which can be approximated by a Gaussian at low T [21]. It is the low T limit we now focus our attention on and we consider two possibilities: either A is a Gaussian or A is a Lorentzian. Considering the latter with a FWHM = Γ and peaked at ω_m and noting that

$$\lim_{T\to 0}\left[\int d\omega\, \xi(t)\right]^r = e^{-r\Gamma t/2}\, e^{ir\omega_m t} \qquad (18)$$

it follows that

$$B_r(\Omega, T=0) = \pi^{-1}\,\mathrm{Re}\left[\int_0^\infty dt\, e^{i(\nu-\Omega+r\omega_m+ir\Gamma/2)t}\right]$$

$$= \frac{r\Gamma/2\pi}{(\Omega-\nu-r\omega_m)^2+(r\Gamma/2)^2} \qquad (19)$$

Thus, with a one-phonon spectrum centered at $\nu + \omega_m$ and possessing a width Γ, the r-phonon spectrum is centered at $\nu + r\omega_m$ with a width of $r\Gamma$. Utilization of a Lorentzian for A likely overestimates the dependence of the linewidth on r relative to a Gaussian, which, for coupling to delocalized phonons, may be a more realistic shape. It is readily shown that for a Gaussian the linewidth of the r-phonon spectrum is $r^{1/2}\Gamma$.

In the following subsection we utilize the $T = 0$ K limit of $G(\Omega)$ (Eqn. 14) to develop the shape of the hole-burned spectrum. The formalism admits any shape for $A(\nu - \Omega)$ but in order to obtain an expression for the hole profile which is simple and physically transparent we will utilize the following single site absorption profile

$$L(\Omega-\nu) = e^{-S}I_0(\Omega-\nu) + \sum_{r=1}^{\infty}\frac{S^r e^{-S}}{r!}I_r(\Omega-\nu-r\omega_m) \qquad (20)$$

Here, I_r is given by Eqn. 19 but for model calculations the width $r\Gamma$ is replaced by $r^{1/2}\Gamma$ so that the second term in Eqn. 20 is a reasonable approximation to a sum of Gaussians, especially for large S

– the case of interest. The zero-phonon line shape is taken as homogeneously broadened with the FWHM of l_0 equal to γ.

Finally, we consider the case where a pseudo-localized or resonant phonon mode [20] associated with the impurity dominates the phonon spectrum and is characterized by strong coupling ($S > 1$). It is well known [22] that the $T = 0$ K absorption spectrum also has the functional form of Eqn. 20 although the linewidths for the r-phonon transitions ($r \geqslant 1$) are determined by resonant relaxation of the r-phonon level into the continuum of delocalized phonons [20] as well as the dispersion in the pseudolocalized phonon frequency due to site inhomogeneity. Thus, our expression for the hole profile can also be utilized for pseudolocalized phonons.

The hole profile

With suitable modifications mandated by strong electron-phonon coupling, our approach follows that of Friedrich et al. [5]. We define $N_0(\nu - \nu_m)/N$ as the probability of finding a site with a zero-phonon transition frequency equal to ν. For amorphous solids or protein environments a Gaussian distribution is usually used but, for reasons already mentioned, we employ a Lorentzian:

$$\frac{N_0(\nu - \nu_m)}{N} = \frac{\Gamma_{inh}/2\pi}{(\nu - \nu_m)^2 + (\Gamma_{inh}/2)^2} \tag{21}$$

for the pre-burn distribution. Given the approximate form of $L(\Omega - \nu)$ (Eqn. 20), utilization of a Lorentzian should introduce little additional error for strong coupling. Let the absorption cross-section, laser intensity and photochemical quantum yield equal σ, I and ϕ, respectively. Then following a burn for time τ [5]

$$N_\tau(\nu - \nu_m) = N_0(\nu - \nu_m)\, e^{-\sigma I \phi \tau l(\omega_B - \nu)} \tag{22}$$

where ω_B is the laser burn frequency and $L(\omega_B - \nu)$ is given by Eqn. 20. To obtain the absorption spectrum, A_τ, following the burn we must convolve Eqn. 22 with $L(\Omega - \nu)$ and integrate over ν. Thus,

$$A_\tau(\Omega) = \sum_{r=0} \frac{S^r e^{-S}}{r!} \int d\nu \times N_0(\nu - \nu_m)\, e^{-\sigma I \phi \tau L(\omega_B - \nu)} l_r(\Omega - \nu - r\omega_m) \tag{23}$$

For simplicity we employ the short-burn-time limit where the exponential can be expanded as $1 - \sigma I \phi \tau L(\omega_B - \nu)$. This approximation need not be made, although the resulting expressions are very cumbersome if it is not. The hole spectrum in the short-burn-time limit is simply

$$A_0(\Omega) - A_\tau(\Omega) = \sigma I \phi \tau \sum_{r,r'=0}^{\infty} \left(\frac{e^{-S} S^r}{r!}\right)\left(\frac{e^{-S} S^{r'}}{r'!}\right) \int d\nu \times N_0(\nu - \nu_m) l_r(\Omega - \nu - r\omega_m) l_{r'}(\omega_B - \nu - r'\omega_m) \tag{24}$$

Because we are interested in holes whose widths are comparable to Γ_{inh} we cannot assume, as in Ref. 5, that $N_0(\nu - \nu_m)$ is constant in Eqn. 24. The convolution of the three Lorentzians can be performed using the method of residues but the procedure is tedious. A far more facile approach is to express each of the Lorentzians as the Fourier transform of the appropriate exponential time decay. Performing the frequency integration ($d\nu$) first yields $2\pi\delta(t + t' + t'')$. Taking due account of the possible time orderings in the time integration immediately yields

$$\begin{aligned}
[A_0 - A_\tau](\Omega) = {} & \frac{\sigma\phi\tau}{3(2\pi)^2}\left(\sum_{r,r'=0}^{\infty} \frac{S^r e^{-S}}{r!} \frac{S^{r'} e^{-S}}{r'!}\right) \\
& \times \left[\left\{ \frac{\Gamma_{inh} + \Gamma_r}{(\Omega - \nu_m - r\omega_m)^2 + \left(\frac{\Gamma_{inh} - \Gamma_r}{2}\right)^2} \right\} \right. \\
& \times \left\{ \frac{\Gamma_r + \Gamma_{r'}}{(\Omega - \omega_B + \omega_m(r' - r))^2 + \left(\frac{\Gamma_r + \Gamma_{r'}}{2}\right)^2} \right\} \\
& + \left\{ \frac{\Gamma_{inh} + \Gamma_{r'}}{(\omega_B - \nu_m - r'\omega_m)^2 + \left(\frac{\Gamma_{inh} + \Gamma_{r'}}{2}\right)^2} \right\} \\
& \times \left\{ \frac{\Gamma_r + \Gamma_{r'}}{(\Omega - \omega_B + \omega_m(r' - r))^2 + \left(\frac{\Gamma_r + \Gamma_{r'}}{2}\right)^2} \right\} \\
& + \left\{ \frac{\Gamma_{inh} + \Gamma_{r'}}{(\omega_B - \nu_m - r'\omega_m)^2 + \left(\frac{\Gamma_{inh} + \Gamma_{r'}}{2}\right)^2} \right\} \\
& \left. \times \left\{ \frac{\Gamma_{inh} + \Gamma_r}{(\Omega - \nu_m - r\omega_m)^2 + \left(\frac{\Gamma_{inh} + \Gamma_r}{2}\right)^2} \right\} \right]
\end{aligned} \tag{25}$$

the desired result. For compactness we have defined $\Gamma_r = \gamma$ for $r = 0$ and $= r^{1/2}\Gamma$ for $r \geqslant 1$, where γ is the damping constant for the zero-phonon transition. Considering the complexity of the problem, Eqn. 25 is simple in form as well as physically transparent. For example, consider strong coupling where $S > 1$ and phonon processes with large r the most probable, r_{max}. Consider next the burn frequency ω_B located in the high-energy tail of the absorption profile where transitions with $r' > r_{max}$ are predominately excited. From the first factor of the second term of Eqn. 25 we have $\omega_B = \nu_m + r'\omega_m$ which when inserted into the second factor of the same term yields the resonance $\Omega - \nu_m - r\omega_m$. The factor $S^r e^{-S}/r!$ favors $r \approx r_{max} < r'$, so that the hole maximum may well be red shifted relative to ω_B. The other two terms indicate a red shift as well. In the same way one can argue that for ω_B in the low-energy tail the hole may be blue shifted relative to ω_B. The extents of these shifts and the value of ω_B for which the hole is coincident are determined by the interplay between S, Γ_{inh} and Γ.

Calculations

In order to simulate spectra Fortran computer programs for calculating the single site absorption (Eqn. 20), the inhomogeneously broadened absorption (the convolution of Eqn. 20 with the site distribution function (Eqn. 21)) and the hole spectrum (Eqn. 25) were written. Input data required for the programs were the one-phonon absorption width, Γ, the one-phonon displacement frequency, ω_m, the excited state lifetime, γ^{-1}, the inhomogeneous width, Γ_{inh}, and the Huang-Rhys factor, S. The effects of varying each of these parameters will be discussed in the following section.

In addition to these parameters the frequency interval at which the spectra were calculated could also be specified. The step size selected is similar to the spectroscopic resolution in experimental spectra, although it is not exactly analogous. If the step size is small compared to the narrowest spectral feature, then the spectra will be undistorted. However, if the step size is comparable to or greater than the width of the spectral features then distortions will occur. In particular, if the step size and starting position are such that calculations are carried out half a step away from a sharp maximum, then the maximum will be diminished relative to the same result obtained with the calculated points shifted half a step so that the value at the maximum is calculated. Although it would be preferable to perform the calculations with a small step size to avoid these distortions, the time required to perform a computation can become quite large. However, the hole spectra were all calculated so that a value was calculated at the peak of the sharp features. The effect of this is that these features are more easily seen in the noise-free calculations than they would be in actual experimental data.

One final point to be made about the calculations is how the infinite sums (or double sums) over multi-phonon processes were handled. In general these sums were performed for $r = 0$ to $r = 20$. The accuracy obtained in truncating at this point is dependent upon the value of S. For $S = 4$, this truncation resulted in neglecting $2 \cdot 10^{-7}\%$ of the intensity at each point. For $S = 8$, 0.009% of the intensity was neglected.

The calculations were performed on a Digital Equipment Corporation VAX-11/780.

Results

Computed profiles

Ultimately the aim of the computer simulations is to compare the computed spectra with experimental spectra and thereby obtain reasonable estimates for parameters such as the Huang-Rhys factor, S, the mean phonon frequency to which the transition is coupled, ω_m, and the inhomogeneous broadening, Γ_{inh}. It is instructive, however, to consider first the various spectral shapes themselves, apart from any experimental data to appreciate the effect of the various parameters on the spectral profiles.

Single site absorption profile. The single site absorption spectrum or profile is not experimentally measurable. Its computed shape, however, does allow the effects of variations in S, Γ, ω_m, and γ to be assessed without the complications introduced by the site inhomogeneous distribution. Fig. 1 illustrates for fixed Γ, ω_m, and γ, the variation in the single site absorption shape as S is consecutively doubled from 0.5 to 8. Since the

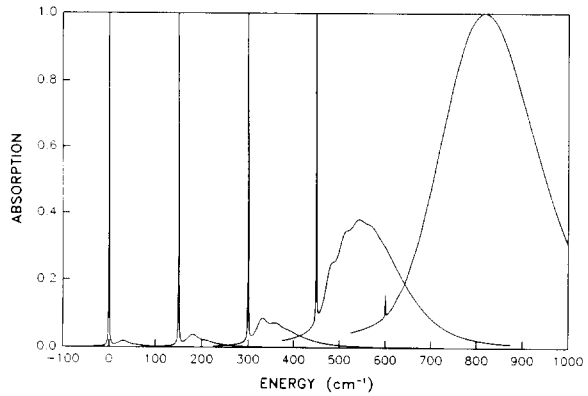

Fig. 1. Single site absorption profiles calculated according to Eqn. 20 with $\Gamma = \omega_m = 30$ and $\gamma = 1$. From left to right the values of S are 0.5, 1.0, 2.0, 4.0 and 8.0. For ease of inspection the $S = 1$ to $S = 8$ spectra are artificially shifted in steps of 150 cm^{-1} relative to the $S = 0.5$ spectrum.

area under each of the bands is equal, as the bands broaden with increasing S the peak intensities decrease by two orders of magnitude. Hence the spectra have been normalized to unity at the frequency of the most strongly absorbing point of the spectrum. In the absence of this normalization it would not be possible to present the five shapes on the same coordinate system. For ease of inspection the spectra for $S > 0.5$ have been shifted in steps of 150 cm^{-1} relative to the $S = 0.5$ spectrum.

From Eqn. 20, it can be seen that the intensity of the zero-phonon contribution to the line shape is e^{-S}. Thus in Fig. 1, the zero-phonon lines are 60.6, 36.8, 13.5, 1.83, and 0.0339% of the total intensity for $S = 0.5$, 1.0, 2.0, 4.0 and 8.0, respectively. Note also, that the peak of the phonon absorption increases with increasing S and is maximum at approx. $S\omega_m$. The width of the phonon wing of the single-site absorption also increases significantly as S increases and is also dependent upon Γ, the one-phonon absorption width.

Convolution with Γ_{inh} – the inhomogeneous absorption profile. To obtain the inhomogeneously broadened absorption spectrum involves the convolution of Eqn. 20 with the site distribution function, Eqn. 21. The resulting absorption shape is

$$A_0(\Omega) = \sum_{r=0}^{\infty} \frac{e^{-S}S^r}{r!} l_{r,\mathrm{inh}}(\Omega - \nu - r\omega_m) \tag{26}$$

where $l_{r,\mathrm{inh}}$ is a Lorentzian with a peak at $\nu + r\omega_m$ and width equal to $\Gamma_r + \Gamma_{\mathrm{inh}}$, where as before $\Gamma_r = \gamma$ for $r = 0$ and $\Gamma = r^{1/2}\Gamma$ for $r > 0$. Since every term of the sum has a width greater than Γ_{inh}, there will be no features sharper than Γ_{inh}. In general, the profile will be structureless unless ω_m is comparable to or greater than Γ_{inh}. In that case, peaks or shoulders with a separation of ω_m will be discernible, although if the phonon absorption widths are large, these features may again be obscured.

The calculated absorption bands are asymmetric, tailing more slowly on the high-energy side. A measure of the degree of asymmetry is the comparison of the full width at half maximum intensity with twice the width measured from the peak frequency to the half maximum intensity point on the low-energy side of the band. Widths measured in the latter manner are as much as 15% narrower than the full widths. The absorption width, Γ_{abs}, is given approximately by

$$\Gamma_{\mathrm{abs}} = \Gamma_{\mathrm{inh}} + S\omega_m \tag{27}$$

Deviations from this relation increase as S increases.

The peak of the absorption can deviate considerably from the peak of the site distribution function. The displacement is approximately $S\omega_m$. This shift can be understood from the single site absorption profiles. The maximum Franck-Condon factor occurs for $S = r$, corresponding to an r-phonon process shifted from the zero-phonon frequency by $r\omega_m$. Thus the frequency at which there is a maximum number of absorbers, i.e., the maximum of the site distribution function, ν_m, will produce an absorption maximum similarly shifted. As will be seen, hole burning results can lead to a determination of ν_m. In conjunction with the inhomogeneous absorption spectrum, this allows determination of $S\omega_m$.

The computed inhomogeneous absorption profiles are used to check that the parameters used for the hole burning simulations produce absorption shapes with asymmetries, widths and peak wavelengths consistent with the experimental absorption shapes.

The hole spectrum. The hole spectrum in the short burn time limit is given by Eqn. 25. Figs. 2

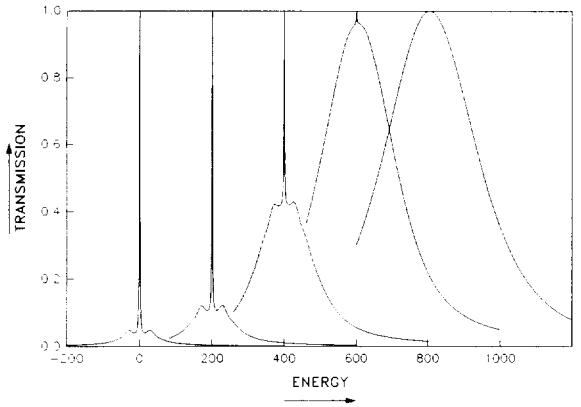

Fig. 2. Hole profiles calculated according to Eqn. 25 with $\Gamma = \omega_m = 30$, $\gamma = 1$, $\Gamma_{inh} = 300$ and $\omega_B = 0$. From left to right the values of S are 0.5, 1.0,2.0, 4.0 and 8.0. The hole profiles are artificially displaced from each other for ease of inspection, see text.

and 3 illustrate holes calculated according to this equation with the same parameters as used for Fig. 1, viz., $\omega_m = 30$, $\Gamma = 30$, $\gamma = 1.0$, and S = 0.5, 1.0, 2.0, 4.0 and 8.0. The additional parameters needed for evaluation of Eqn. 25 are the burn frequency, ω_B, and the inhomogeneous distribution width, Γ_{inh}. For both Fig. 2 and Fig. 3, $\Gamma_{inh} = 300$ was used. In order to display the holes on a single coordinate system, the distribution maxima were taken as $\nu_m = 0$, 200, 400, 600 and 800 corresponding to $S = 0.5$, 1.0, 2.0, 4.0 and 8.0, respectively. The corresponding burn frequencies

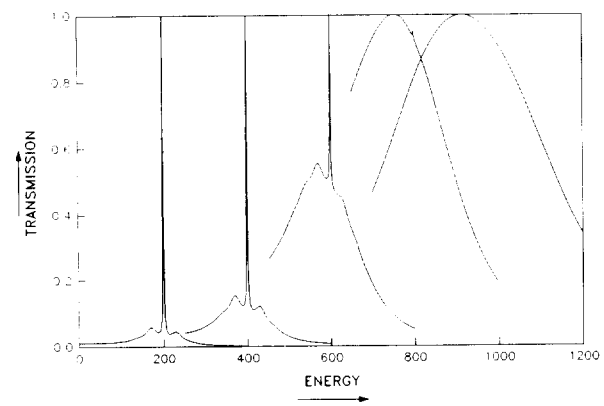

Fig. 3. Hole profiles calculated according to Eqn. 25 with $\Gamma = \omega_m = 30$, $\gamma = 1$, $\Gamma_{inh} = 300$ and $\omega_B = \nu_m + 200$. From left to right the values of S are 0.5, 1.0, 2.0, 4.0, and 8.0. Hole profiles are artificially displaced from each other for ease of inspection.

were $\omega_B = \nu_m$ for Fig. 2, and $\omega_B = \nu_m + 200$ for Fig. 3.

Comparison of Fig. 1 and Fig. 2 reveals several interesting features. First, while the single site line shapes show phonon absorption primarily to the high energy side of the zero-phonon line, the hole spectra have phonon wings to both higher and lower energy. As shown in Fig. 2, the holes burnt at $\omega_B = \nu_m$ have a phonon structure that is nearly symmetric about the zero-phonon hole. For holes burnt with $\omega_B > \nu_m$ (the distribution maximum), the phonon wings are skewed toward ν_m, as shown in Fig. 3. Skewing in the opposite direction occurs for $\omega_B < \nu_m$. The influence of the position of the excitation frequency within the homogeneous distribution has previously been noted by Kikas [23], with regard to line narrowed fluorescence spectra in which only a low energy phonon band occurs.

There are a number of reports which experimentally confirm the presence of both high and low energy phonon holes [5,24,25]. The low energy phonon wings are understood to originate primarily from the burning of zero-phonon features of sites at energies lower than ω_B, which have been excited through phonon absorption. The higher energy phonon hole consists of the phonon wings of sites which absorb through their zero-phonon line plus a contribution from the tails of the phonon wings of lower energy sites. This summing of the tails of lower energy sites is responsible for the slight asymmetry which is revealed by close examination of the holes of Fig. 2. Fig. 3 of Ref. 25 is an example of nearly symmetric high- and low-energy phonon holes. The preponderance of published hole spectra in which the low energy phonon hole is predominant indicates that these holes were burnt at energies higher than the energy of the peak of the site distribution function.

The ratio of zero-phonon hole to the total hole intensity is (from Eqn. 25) e^{-2S} at $\omega_B = \nu_m$. This is in contrast with the corresponding ratio for the single-site absorption given above: e^{-S}. For the hole spectra this ratio is not constant but varies with the position of ω_B within the inhomogeneous distribution. From Eqn. 25 it can be seen that all the frequency terms in the denominators disappear for $r = r' = 0$ when $\Omega = \omega_B = \nu_m$. This produces the zero phonon hole at ω_B. However, when $\omega_B \neq \nu_m$, these terms do not disappear and cause a

reduction in the intensity of the zero-phonon hole relative to the total hole intensity. This effect is most easily seen by comparing the hole shapes for $S = 4$ in Fig. 2 with the corresponding hole in Fig. 3, in which the zero-phonon hole is noticeably less intense. It should be emphasized that this decrease of the zero-phonon hole intensity is easily seen in the computed spectra where the spectra are all normalized to unity. Experimentally, the effect may be partly obscured by the variation in hole depth due to differences in absorption throughout the inhomogeneous profile.

Note in Fig. 2 and 3, that for $S = 8$ no zero phonon hole is detectable. For this S-value the zero-phonon feature would carry e^{-16} of the total intensity, i.e., $1 \cdot 10^{-7}$. Certainly, such weak features would be impossible to detect experimentally. Comparison of Fig. 2 with Fig. 3 for $S = 8$ shows that the hole has broadened considerably as the burn frequency shifts from ν_m to $\nu_m + 200$. This broadening is due to their being two dominant features in the hole spectrum: one which occurs at ν_m and the other which occurs at ν_B. The large number of absorbers at ν_m will make a major contribution to the hole spectrum even when these absorbers are only being excited through phonon side-band absorption. The more strongly absorbing molecules with zero-phonon absorptions at ν_B will also make a strong contribution to the hole shape. As these two contributions separate from each other the hole appears to widen until the separation is approximately equal to the widths of the two features. Since the widths will be on the order of Γ_{inh}, separate features may not be discernible until $\omega_B = \nu_m \pm 300$, or greater. Experimentally, such large shifts may be into a very weakly absorbing region, producing negligible holes.

Comparison of calculated and experimental profiles for primary electron donor states

On the basis of the hole-burning results (see Introduction) of Maslov et al. [8] on P-700 of a PS I and Boxer et al. [10,12] and Wiersma et al. [11,13] on P-870 and P-960 of *Rb. sphaeroides* and *Rps. viridis,* one would conclude that the two primary electron donor states of the bacterial systems differ in a very substantive way from P-700. Again, Maslov and coworkers observed only a sharp zero-phonon hole coincident with ω_B which is two orders of magnitude sharper than the approx. 400 cm^{-1} wide holes observed for P-870 and P-960. The hole-burning studies of Boxer and coworkers on P-870 and P-960 are more extensive than those of Wiersma and coworkers and show that there is an interesting dependence of the broad hole profile on ω_B (see Introduction and below). The later more detailed studies of Gillie and coworkers [9] on P-700 of enriched PS I particles from spinach revealed that the hole profile is comprised of a weak but sharp (approx. 0.05 cm^{-1}) hole superimposed on an intense broad hole whose width is comparable to those observed for P-870 and P-960. With this work it would appear that the differences between the hole-burning characteristics of P-870 (P-960) and P-700 may not be so great.

In what follows it will be shown that the hole-burning and complementary characteristics, such as the Stokes shift and thermal broadening, of the three primary electron donor states are consistent with strong linear electron-phonon coupling and a significant site inhomogeneous broadening contribution to the low temperature absorption profile. At this point, the absence of a sharp zero-phonon hole in the spectra of P-870 and P-960 should only be viewed as consistent with strong electron-phonon coupling and site inhomogeneous broadening. The calculations indicate that under optimum experimental conditions the zero-phonon hole may be observable. In the same vein, it is the presence of the broad intense hole in the spectra of P-700 which is, at this time, more important than the observation of the weak zero-phonon hole. It will be seen that the variations in the parameters of Eqn. 25 required to account for the principal differences in the hole spectra for the three primary electron donor states are not, in any profound sense, significant.

P-870 and P-960. Previously we have shown that the P-870 hole-burning data [10,11] for *Rb. sphaeroides* can be explained by Eqn. 25 [17] with appropriate choice of the parameters S, ω_m, Γ_{inh}, Γ, γ and ν_m. In this subsection we present a more detailed comparison of the experimental results with the calculated hole shapes for P-870 and P-960 of *Rps. viridis.* Ideally, hole burning, Stokes shift and thermal broadening data (associated with

the absorption and fluorescence origin profiles) should suffice to fix the values of most of the above parameters. We proceed to discuss the determination of these parameters and the difficulties associated therewith when a zero-phonon hole coincident with ω_B is not observable (as is the case for P-870 and P-960).

For holes burnt on the low-energy side of the absorption profile, Eqn. 25 shows that the broad hole maximum will occur near the maximum, ν_m, of the zero-phonon site distribution function. When $\omega_B = \nu_m$, the broad hole maximum will coincide with ω_B. The displacement between the absorption profile maximum and ν_m is approx. $S\omega_m$. Furthermore, the Stokes shift is approx. $2S\omega_m$ so that one has an important check on the value of $S\omega_m$ determined from hole burning.

Calculations with Eqn. 25 also show that slight variations in the position of the broad hole maximum with variations in ω_B will be observable when $\Gamma_{inh} \gtrsim S\omega_m$. These variations are observed for P-870 [10] but not for P-960 [12]. Thus, it would appear that Γ_{inh} (P-960) < Γ_{inh}(P-870). We return to this point shortly when the thermal broadening data are discussed.

When phonon structure is not observable in the absorption or hole spectra, thermal broadening data can be used to determine the mean phonon frequency ω_m. The linear electron-phonon coupling contribution to the width of the absorption profile is [19]

$$\tilde{\Gamma}(T) = \left(S\omega_m^2 \coth\frac{\hbar\omega_m}{2kT}\right)^{1/2} \tag{28}$$

Use of Eqn. 28 to determine ω_m is complicated by the fact that Γ_{inh} is also a contributor to the absorption linewidth, Γ_{abs}. When the absorption profile is assumed to be a Gaussian, the method of moments [18,19] yields

$$\Gamma_{abs}(T) = \left(\tilde{\Gamma}(T)^2 + \Gamma_{inh}^2\right)^{1/2} \tag{29}$$

for the T-dependent absorption linewidth. However, the assumption of a Gaussian is not sufficiently accurate because of the asymmetries associated with the P-870 and P-960 absorption profiles. Calculations with Eqn. 26 yield the relationship

$$\Gamma_{abs}(T) \approx \tilde{\Gamma}(T) + \Gamma_{inh} \tag{30}$$

The thermal broadening data for the P-870 and P-960 absorption profiles are consistent with Eqn. 30. In Fig. 4 is shown the absorption spectra for the reaction center of *Rb. sphaeroides* and *Rps. viridis* in an ethylene glycol/water glass at 1.6 K. For this solvent, the P-870 and P-960 absorption profiles are particularly well separated from their respective bacteriochlorophyll monomer absorptions at 800 and 835 nm, respectively. Thus, accurate thermal broadening studies on the primary electron donor states are possible. The results of such a study are shown in Fig. 5. Aside from an approx. 210 cm^{-1} offset, the thermal broadenings of P-870 and P-960 are identical within experimental error. The same behavior has been observed by Holten and Kirmaier (unpublished data)

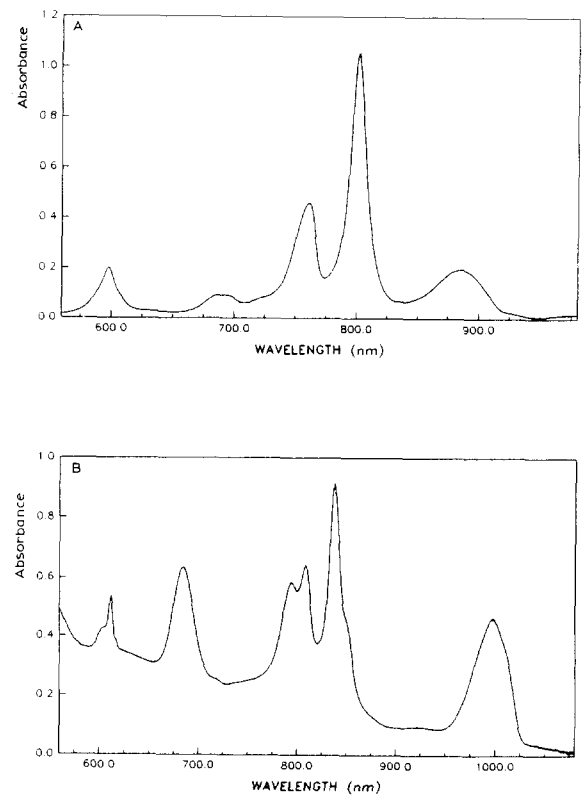

Fig. 4. Absorption spectra of reaction centers preparations from (A) *Rb. sphaeroides* and (B) *Rps. viridis*, both in an ethylene glycol/water glass at 1.6 K.

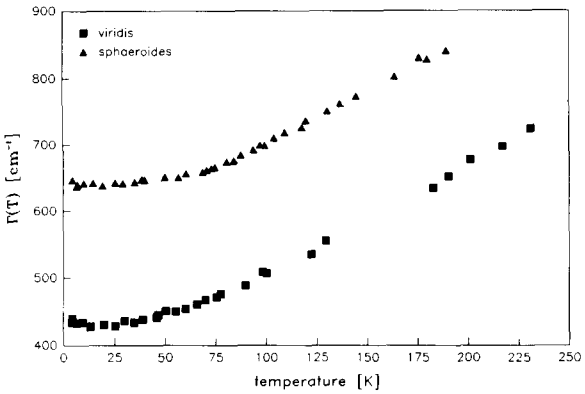

Fig. 5. Thermal broadening of the P-870 and P-960 primary electron donor bands of *Rb. sphaeroides* and *Rps. viridis* in an ethylene glycol/water glass. Γ corresponds to the full-width at half-maximum.

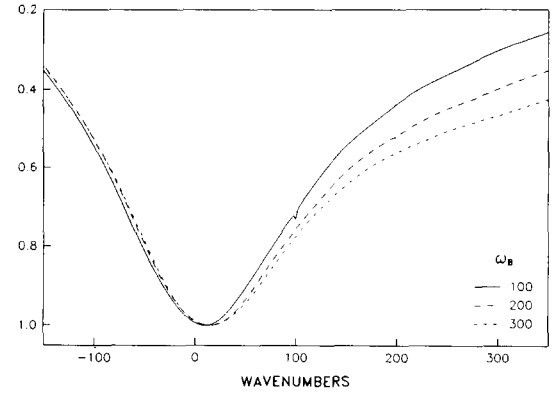

Fig. 6. Hole spectra for P-870 calculated according to Eqn. 25 with the parameters given in Table I.

who employed poly(vinyl alcohol) and gelatin films as low-temperature matrices. Although solvent perturbations on the width and position of the primary electron donor state absorption profile exist, it is generally the case that the width of P-870 is substantially greater than that for P-960. From Fig. 5 we can conclude that Γ_{inh}(P-870) $\approx$ Γ_{inh}(P-960) + 210. However, in order to analyze the data of Fig. 5 with Eqn. 28 so that ω_m can be determined, a value for Γ_{inh}(P-960) is required. As Γ_{inh}(P-960) increases, ω_m decreases. Our determination of Γ_{inh}(P-960) will rest on the quality of fit of Eqn. 25 to the hole burning data. However, we note that the linear electron-phonon coupling of chlorophyll monomers is weak [26] as has recently been determined for the core antenna complex C-670 of PS I [14]. Thus, the widths of B800 and B835 in Fig. 4a and b as well as those for the bacteriopheophytin monomer serve as a rough guide for Γ_{inh}(P-960). Of course, each of these 'monomer' bands is contributed to by two identical pigments associated with the L and M protein arms of the reaction center [27,28]. Inequivalent protein interactions for *Rps. viridis* are sufficient to produce a splitting of the bacteriopheophytin *b* band at 800 nm (Fig. 4b). Moreover, the Q_y states of the pigments in the reaction center are to a modest extent mixed by excitonic interactions [29]. Nevertheless, from the 'monomer' transitions in Fig. 4a and b, Γ_{inh} values in the range 150–350 cm^{-1} can be estimated. This range is consistent with the Γ_{inh} values for C-670 and P-700 of PS I, see following subsection.

Reasonable fits with Eqn. 25 to the hole-burning data of Boxer and coworkers on P-870 [10] and P-960 [12] are obtained for the parameter values given in Table I. The calculated curves for P-870 are shown in Fig. 6 where the burn frequencies are given relative to $\nu_m \equiv 0$ (maximum of the site distribution function) and chosen to be similar to the burn frequencies used in the experiment. For $S = 4$, the zero-phonon hole carries only 0.03% of the total hole intensity for $\omega_B \approx \nu_m \equiv 0$. It is discernible for the $\omega_B = 0$ and -100 cm^{-1} curves, but is less so for the $\omega_B > 0$ curves because of the diminishing contribution from zero-phonon transitions to the absorption relative to that from multi-phonon transitions as ω_B increases past ν_m. The signal to noise and resolution of the experiments in Refs. 10, 12 would preclude observation of the weak zero-phonon hole. On the other hand, for S as small as 2, a zero-phonon hole would be

TABLE I

PARAMETERS USED TO CALCULATE HOLE SPECTRA FOR THE VARIOUS REACTION CENTERS

For comparison, values for the core antenna complex C-670 of PS I are also included.

	Γ_{inh}	Γ	γ	S	ω_m
P-960	150	40	1.0	4.5	80
P-870	350	50	2.5	4.5	80
P-700	300	30	0.06	5.5	30
C-670	200	40	0.03	< 0.9	30

easily detectable for the γ value given in Table I. In Fig. 6, the displacements between the broad hole maximum and ω_B and the increase in the broad hole width with increasing ω_B are consistent with the experimental data [10,12]. As discussed in Ref. 17, the broadening and shifting of holes in *Rb. sphaeroides* is due to the superposition of two broad holes. One of these holes is due to burning of the large number of sites at ν_m which contribute through phonon absorption even when ω_B is quite remote from ν_m. This hole does not shift. The other hole is coincident with ω_B and therefore changes with changes in ω_B. The contribution of these two terms is easily seen in the calculations when ω_B is shifted more than Γ_{inh} from ν_m. This effect is evident in Fig. 3 of Ref. 17. The effect is much more difficult to see experimentally, due to overlapping absorptions when ω_B is shifted to higher energy of ν_m and due to very weak absorption when shifted to lower energy.

To what extent are the parameter values in Table I for P-870 consistent with the various types of experimental data? First, the differences between the hole spectra of P-870 and P-960 (see below) are accounted for by a value of Γ_{inh} (P-870) which is substantially greater than the value for Γ_{inh} (P-960) (as required by the data of Fig. 4 and those of Holten and Kirmaier (unpublished data)). Second, the measured Stokes shift for P-870 is approx. 500 cm^{-1} [18,27] which should be compared with $2S\omega_m \approx 640$ cm^{-1} (from Table I). The agreement is reasonable considering the experimental uncertainties. Furthermore, 500 cm^{-1} would be a lower limit for $2S\omega_m$ if the P-870 fluorescence is not thermally relaxed with respect to phonons or if small depressions in phonon mode frequencies occur in the excited state. Third, for Γ_{inh}(P-870) $\approx$ 350 cm^{-1}, the thermal broadening data of Fig. 5 are well accounted for by Eqns. 28 with $\omega_m = 108$ cm^{-1}. This frequency (mean) is associated with the ground electronic state. In setting $\omega_m = 80$ cm^{-1} a frequency depression of approx. 20% is assumed for the excited electronic state. Fourth, no direct measurement of the one-phonon profile width, Γ, is possible due to the large Huang-Rhys factor S. However, a value of $\Gamma \approx 40$ cm^{-1} has recently been measured for C-670 of PS I [14]. Furthermore, fluorescence-line-narrowed spectra of aromatic molecules imbedded in low T glasses typically exhibit Γ values in the range 20–50 cm^{-1}. The calculated spectra of Fig. 6 are only slightly altered by decreasing Γ from 50 to 30 cm^{-1}. At 30 cm^{-1} phonon sideband progressional structure, not noticeable in the experimental data, begins to appear. There is also a slight decrease in the hole width.

We turn now to P-960 of *Rps. viridis* which also exhibits broad holes whose widths are similar to those observed for P-870. However, the shifting of the hole maximum and variation of the hole-width with ω_B appear to be absent for P-960. This can be understood if Γ_{inh}(P-960) is significantly less than Γ_{inh}(P-870) as required by Fig. 5. Given the similarity [28,30] in the reaction center structures for *Rb. sphaeroides* and *Rps. viridis*, the identical thermal broadening characteristics for P-870 and P-960 (vide supra) are reasonable. The calculated hole spectra for P-960 obtained with the parameter values given in Table I are shown in Fig. 7. The values for S and ω_m are the same as those used for P-870 but Γ_{inh}(P-960) is reduced to 150 cm^{-1}. Note that with $\Gamma = 40$ cm^{-1} some phonon progressional structure is evident on the high-energy side of the holes. Increasing Γ to approx. 50 cm^{-1} smears out this structure while only increasing the hole width 10–20 cm^{-1}. Fig. 7 shows that the broad hole maximum frequency is essentially insensitive to variations in ω_B as observed [12]. Furthermore and very importantly, the holes are nearly identical on the low-energy side while exhibiting deviations on the high-energy side which is also in accord with the experimental

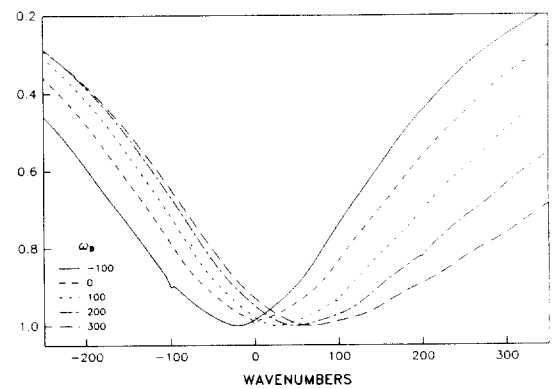

Fig. 7. Hole spectra for P-960 calculated according to Eqn. 25 with the parameters given in Table I.

spectra [12]. Fig. 7 indicates that under the appropriate conditions (high signal-to-noise ratio, $\omega_B \approx \nu_m \equiv 0$ and adequately high burn and reading resolutions) that a weak zero-phonon hole for P-960 should be observable. Although the agreement between these calculations and the data of Ref. 12 is perhaps less satisfying than the agreement of the experimental and calculated P-870 data, the main trends of Ref. 12 are observed. At least in part, the deviation between calculated and experimental holes is attributable to requiring that the zero phonon hole be absent from the calculated holes in agreement with the experimental result. This was done while at the same time doing the calculations at a higher resolution than actually used in the experiments. In Refs. 12 and 13 laser line widths of approx. 2 cm^{-1} were used. These line widths would result in an effective value for γ of approx. 4 cm^{-1}, rather than the value of 1 cm^{-1} used in the calculations which is consistent with the lifetime of P-960.

P-700 of PS I. An example of a hole burned spectrum for P-700 of enriched (approx. 35 : 1) PS I particles from spinach chloroplast is shown in Fig. 8 [9]. Superimposed on the broad hole is a weak but sharp zero-phonon hole coincident with ω_B. Such profiles have been observed for $700 \leqslant \lambda_B \leqslant 720$ nm. Recent very high resolution (approx. 0.002 cm^{-1}) measurements have shown that the zero-phonon holewidths is approx. 0.05 cm^{-1} [14], which is a factor of 2 narrower than the value reported in Ref. 9 where the read resolution used was lower. The implications of the zero-phonon holewidth are considered later. In Fig. 8 the increase in absorption at approx. 14540 cm^{-1} is most likely due to electrochromic shifts of the core antenna chlorophyll absorptions resulting from the reaction center charge separation process [31,32]. The presence of the intense broad hole whose width is comparable to those observed for P-870 and P-960 immediately indicates that the linear electron-phonon coupling for P-700 is also very strong. Unfortunately, theoretical calculations cannot be guided by temperature-dependent absorption and fluorescence data for P-700 due to spectral interference from the core antenna state C670. Reliable P-700 Stokes shift data are also not available. Nevertheless, reasonable agreement with the P-700 hole burning data [9] was achieved with

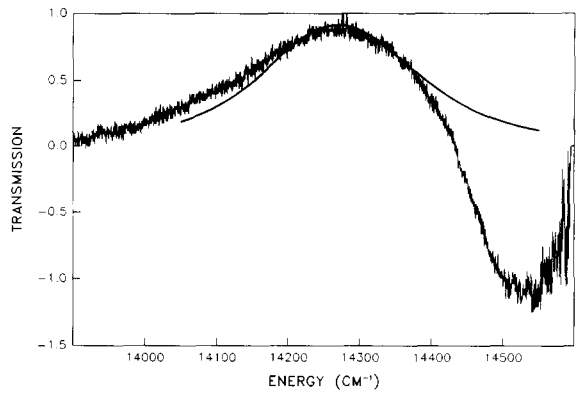

Fig. 8. Calculated and experimental hole spectra for P-700. The calculated spectrum has been shifted 30 cm^{-1} to lower energy, so that the zero phonon holes of both spectra can be seen. The experimental hole was produced by burning for 10 min with 100 $\mu W \cdot cm^{-2}$ at 14284 cm^{-1}.

Eqn. 25 for $S = 7$, $\omega_m = 30$ cm^{-1}, $\Gamma = 30$ cm^{-1}, $\Gamma_{inh} = 300$ cm^{-1} and $\gamma = 0.06$ cm^{-1} [9].

As discussed earlier, Eqn. 25 predicts that the intensity ratio of the zero-phonon to phonon hole is given by e^{-2S}. In Ref. 9 the expression e^{-S} was inadvertently used which yielded $S = 7.1$ from the measured ratio of 1 : 1200. Utilization of the correct expression obviously yields $S = 3.5$. This value with the other parameters fixed at the values used in Ref. 9 yields hole spectra with phonon progressional structure which should be (but is not) observable under the experimental conditions of Ref. 9. At this time we are reticent to change the values of $\omega_m = 30$ cm^{-1} and $\Gamma \approx 30$ cm^{-1}, since a direct measurement of the one-phonon profile for C-670 (albeit a different state) yields these values within experimental uncertainty. The value of $\Gamma_{inh} \approx 300$ cm^{-1} will also be maintained, since the C-670 absorption profile, which exhibits barely but, nevertheless, discernible structure due to chlorophyll *a* pigments in different environments, can be fit with Gaussian profiles with widths of approx. 300 cm^{-1} [33]. With these parameters set, the experimental P-700 hole profile can be fit for $S \approx 5$ or 6 (Table I) (Fig. 8). This increase in S beyond the value of 4 is not unreasonable since Eqn. 25 is only valid for the short burn time limit (where experimental measurements are difficult to make). Thus, the value of S determined with e^{-2S} and the data must be viewed as a lower limit [14]. With the

parameter values of Table I, the calculated spectrum is in reasonable agreement with the experimental spectrum.

Discussion

The theoretical approach taken here satisfactorily accounts for the principal characteristics of the photochemical hole spectra of the P-700, P-870 and P-960 primary electron donor states. The calculations indicate that the linear electron-phonon coupling for all three states is very strong ($S \gg 1$) and that the site inhomogeneous broadening contribution to the absorption profile is large, Table I. For P-870 and P-960, the interplay between the hole burning, thermal broadening and Stokes shift data for determination of S, ω_m and Γ_{inh} was essential. The interrelationships between these types of data were not taken into account in the earliest interpretations of the hole-burning data [10–13].

As improved and more complete data sets become available the values for S, ω_m and Γ_{inh} given in Table I will undergo refinement but not to the extent which would negate the two principal conclusions stated above. Of possible concern is that the value of $\omega_m = 80$ cm^{-1} for P-870 and P-960 was determined primarily from the thermal broadening data for the ethylene glycol/water glass while the hole burning experiments of Boxer and coworkers [10,12] were performed using poly(vinyl alcohol) (PVOH) films. However, the thermal absorption broadening characteristics of P-870 and P-960 in gelatin and PVOH films are (Holten, D. and Kirmaier, C., unpublished data) are very similar to those shown in Fig. 5. This, even though the absorption peak positions and residual low T widths exhibit a measureable dependence on the host (e.g., Γ_{abs}(P-960) = 494 cm^{-1} in gelatin, Γ_{abs}(P-870) $\approx$ 600 cm^{-1} in PVOH). The dependence of Γ_{abs}(0 K) on host solvent indicates a dependence of Γ_{inh} on host due to solvent perturbation of the special pair. To our knowledge, however, a correlation between the magnitude of Γ_{inh} and the nature (strength) of the electron-phonon coupling has not been observed for any molecular system. Therefore, the conclusions that ω_m is insensitive to the host and that ω_m is determined by the special pair-protein complex are reasonable. A related question is why Γ_{inh}(P-870) appears generally to be greater than Γ_{inh}(P-960) for a given host. The answer may involve solvent penetration, since the special pair of *Rps. viridis* is 'capped' by cytochrome *c* [28], whereas this is not the case for *Rb. sphaeroides* [30]. If so, the disparity in Γ_{inh} is of no biological significance although it should be noted that a consideration of the energetic inequivalence of the two monomers of the special pair is necessary for the interpretation of data which speak to excitonic effects of the special pair. That is, in addition to the inequivalence resulting from interactions with the protein environment a contribution from solvent may be necessary. On the other hand, the disparity in Γ_{inh} may be a consequence of a varying degree of intrinsic disorder in the isolated reaction center of the two bacterial systems.

The values of 50 and 40 cm^{-1} for Γ of P-870 and P-960, Table I, deserve some comment. They cover a reasonable range based on the fluorescence line narrowed and hole-burned spectra of a large number of chromophores imbedded in glass and polymer hosts and the direct measurement of $\Gamma \approx 40$ cm^{-1} for C-670 [14] (Table I). However, little significance should be attached to the difference in Γ between P-870 and P-960, since the value of Γ for P-960 can be increased to approx. 50 cm^{-1} without significantly affecting the calculated hole spectra (increasing Γ leads to slight additional hole broadening).

Before discussing the P-700 results it is appropriate to consider the underlying assumptions of the theory. First, it is based on the linear coupling approximation. Second, the one-phonon profile is characterized by a single maximum (mean phonon frequency, ω_m). Third, the r-phonon profiles are described as Lorentzians with a width $\Gamma_r = r^{1/2}\Gamma$ for $r \geq 1$. The Lorentzian assumption is made so that a physically transparent analytic hole shape function can be obtained. Even though r-phonon profiles are probably more accurately described by an asymmetric Gaussian (tailing more slowly on the high energy side), the essential characteristics for the case of coupling to the continuum of phonons, such as the dependence of the broad hole maximum and width on ω_B, are not significantly affected by the utilization of

Lorentzians. The employment of the Gaussian relationship $\Gamma_r = r^{1/2}\Gamma$ with a Lorentzian serves to mimic a Gaussian behavior for the width of the 2- and higher-phonon profiles. On the other hand, the theory is also valid for the case where the one-phonon profile is associated with a pseudo-localized mode at ω_m. Now Γ is determined by the distribution in values of ω_m (from disorder) and a homogeneous contribution from harmonic relaxation of the pseudolocal model into the continuum of bath phonons [20]. When the latter is dominant, a Lorentzian for the one-phonon profile would be appropriate. The second assumption is consistent with the majority of one-phonon profiles observed in the fluorescence line narrowed and hole burned spectra of molecules imbedded in glasses and polymers and the one-phonon profile observed for C-670 [14]. Nevertheless, the theory is readily modified to take into account a multi-peaked one-phonon profile. We have done this and performed calculations with a bimodal distribution (ω_{m_1}, ω_{m_2}). The total Huang-Rhys factor S is $S_1 + S_2$ with a contribution from both components. As expected (because of the additional adjustable parameters), better agreement is obtained especially for P-960. However, until independent confirmation of bimodal structure is obtained, it would be premature to present these results. The first assumption means that the quadratic electron-phonon coupling, which defines the changes in phonon frequencies upon pigment excitation, has been neglected. Provided these are not large ($\lesssim 20\%$), Eqn. 25 is still accurate. However, the quadratic coupling can contribute to the thermal broadening of the absorption (fluorescence) profiles [18,19]. In the harmonic approximation it alone governs the temperature dependence of the absorption maximum [18,19]. We have performed detailed studies of the lineshift for both P-870 and P-960 (ethylene glycol/water glass). Both absorption bands exhibit a significant blue shift with increasing temperature which is adequately fit by the quadratic coupling expression $\omega_l^2(\delta_l^2 - 1)(4\omega_l)^{-1} \coth(\hbar\omega_l/2kT)$, where ω_l is the ground-state phonon frequency [18] and where $\delta_l = \omega_l'/\omega_l$, with ω_l' the frequency for the excited electronic state. It is found that $\omega_l = 84$ and 124 cm^{-1} and $\omega_l' = 193$ and 273 cm^{-1} for P-870 and for P-960, respectively. These values are in reasonable agreement with those obtainable from the data of Holten and Kirmaier (unpublished data) on P-870 in PVOH and P-960 in a gelatin film. We note first that it is difficult to understand how low-frequency modes could undergo such dramatic increases in frequency. Second, our calculations show that the thermal broadening from the sequence structure from such modes combined with a contribution from the linear electron-phonon coupling are inconsistent with the thermal broadening data. We conclude, therefore, that the thermal lineshifts of P-870 and P-960 arise from the anharmonic terms which affect the thermal expansivity of the reaction center but do not contribute significantly to the thermal broadening. We note that the lineshifts associated with the bacteriochlorophyll and bacteriopheophytin monomer absorption bands, Fig. 4a and b, are negligible between 4 and approx. 200 K (limit of our experiments). This suggests that the special pair geometry may have a significant dependence on the thermal expansivity.

We consider next the results for P-700 and C-670 (Table I). For C-670 the direct observation of the one-phonon profile building on the zero-phonon established that the linear coupling is weak ($S < 0.9$) [14]. The implication of this for excitation transport from the core antenna to P-700 is discussed elsewhere [14]. More important for this paper is that a direct measurement of $\omega_m \approx 30$ and $\Gamma \approx 40$ cm^{-1} for C-670 was possible. The $\omega_m = \Gamma = 30$ cm^{-1} values for P-700 were used in our earlier calculations [9], which preceded the C-670 studies. In view of the C-670 results, these values for P-700 are preserved in this paper, although it should be emphasized that ω_m for C-670 and P-700 could, in principle, be different. The lack of reliable Stokes shift and thermal broadening data for P-700 is unfortunate, since, as emphasized earlier, they provide a valuable check on the ω_m value. With ω_m and Γ fixed, the determination of S for P-700 was dictated by the observation of a zero-phonon hole and its weak intensity relative to the broad hole whose width is comparable to those observed for P-870 and P-960. The sharpness of the zero-phonon hole (approx. 0.05 cm^{-1} [14]) means that S cannot be reduced as low as 4, since for this value it would be too intense (peak height) in comparison with the ex-

perimental spectra. Maslov et al. [8] have noted that the zero-phonon hole for *Chlamydomonas reinhardtii* cannot be burned when the burning is preceded by a white light bleach of P-700 at low temperature. This suggested that the sharp hole is associated with electron transfer from P-700 [8]. Nevertheless, one cannot exclude the possibility that the sharp hole is not due to P-700 but rather long-wavelength absorbing chlorophyll *a* species which are strongly coupled to the reaction center. The reason for mentioning this is that the zero-phonon holewidth provides a lower limit for electron transfer from P-700 to A_0 (primary acceptor of PS I) of approx. 200 ps [14]. In view of the time-domain studies [34,35] of the *T*-dependence of electron transfer from P-870, this result is surprising. These studies show that the transfer time decreases by a factor of approx. 2 in going from room temperature (where the value is approx. 5 ps) to cryogenic temperatures. Recent time domain studies have yielded values of 10 ps [36] and 2.8 ps (Owens, T.G., Webb, S.P., Mets, L., Alberte, R.S. and Fleming, G.R., unpublished results [37]) for P-700 at room temperature. However, care must be taken when comparing the time domain and hole-burning data. The zero-phonon holewidth could reflect the dynamics of the zero-point level of P-700, whereas the states initially prepared in the time domain experiments form a multi-phononic distribution. Provided that (i) thermalization of protein bath phonons is not completely prior to electron transfer and (ii) the nuclear barrier associated with electron transfer is larger than typical phonon frequencies (approx. 30 cm^{-1}), the low temperature hole burning result can be qualitatively understood. However, the preliminary results of our very recent hole-burning experiments following chemical and white light bleaching of P-700 indicate that the sharp zero-phonon hole is not associated with P-700 that is photoactive at liquid helium temperature (in contradiction with results of Maslov et al. [8]). More extensive experiments of this type are in progress. These recent bleaching experiments do confirm that the broad intense hole is due to photoactive P-700 so that our conclusion that P-700 is characterized by strong electron-phonon coupling is unaltered.

As noted in the Introduction, the nature of the phonons which are active in the primary electron donor state absorption (hole burning) is not known. Two possibilities are: spatially delocalized modes associated with the protein complex and highly localized modes associated with the special pair (e.g., intra-dimer monomer $\cdots$ monomer stretch). We tentatively favor the former, since for P-870 approx. 80 cm^{-1} phonons have been implicated as the key Franck-Condon nuclear tunneling modes associated with electron transfer to the bacteriopheophytin monomer as well as in the subsequent reduction of the quinone [15]. In addition, approx. 30 cm^{-1} phonons have been observed for the chlorophyll *a* monomers of C-670 [14] and have been implicated as the key acceptor modes for excitation transport from C-670 to P-700 [14]. Thus, low-frequency phonons also appear to be active in processes involving pigment monomers. Of course, for the special pair the distinction between protein and dimer modes can be artificial if dynamical mixing is significant (due to their comparable frequencies).

The question of why the linear electron-phonon coupling is strong for P-700, P-870 and P-960, but weak for C-670 (and chlorophyllic monomers in matrices [26]) is very important. High-resolution optical data on a large number of molecular crystals have shown that Huang-Rhys factors as large or greater than approx. 4 generally exist only for excited states which possess significant charge-transfer character, e.g., the charge-transfer state of π-molecular donor-acceptor complexes [38]. This was the basis for an earlier conclusion [17] that the primary electron donor states P-870 and P-960 possess significant charge-transfer character in addition to neutral excitonic character. Significant charge-transfer character is consistent with the theoretical findings of Warshel and Parson [39,40] who consider mixing of the pure charge-transfer states of the dimer with the neutral excitonic state. Since then, this conclusion has been supported by Stark results which revealed that the permanent excited state dipole moment of P-870 [41,42] is large (7–8 D) and roughly parallel to the Mg $\cdots$ Mg axis of the special pair. Since it is difficult to conceive of a way in which a monomer can support significant charge-transfer character for its Q_y state, it has been suggested that P-700 is also a special pair [9], a point of continu-

ing controversy (Ref. 43 and references therein).

Finally, we comment on the differences between the interpretation put forth here for the primary electron donor state hole spectra and that of Meech et al. [13]. The interpretation initially favored by Boxer and coworkers [10] is similar to that presented in Ref. 13. Within this qualitative model the large hole-widths (approx. 400 cm^{-1}) for P-870 and P-960 is ascribed to homogeneous broadening resulting from an ultra-fast (approx. 25 fs) charge-separation process which precedes electron transfer to the bacteriopheophytin. The initially prepared primary electron donor state is viewed as a neutral excitonic state that decays primarily into an intra-dimer charge-transfer state. Subsequent to this, evolution to an interdimer state involving a BChl monomer is postulated to occur. Electron-phonon (vibration) coupling and inhomogeneous line broadening were not taken into account and calculated hole spectra were not presented [13]. Very recently [44] Won and Friesner have taken both of these effects into account in a model in which the initially prepared state (P-870 and P-960) is viewed as a mixed state with significant charge-transfer character (within the adiabatic Born-Oppenheimer approximation). Thus, there are definite similarities between their model and ours [17] which we have considered in detail here. However, a major difference stems from the fact that Won and Friesner assume that the electron-phonon (and vibration) coupling is weak which means that the absence of a sharp zero-phonon hole in their calculated spectra for P-960 is due to a breakdown of the Born-Oppenheimer approximation associated with ultra-fast decay of the primary electron donor state into charge-separated states of the reaction center. It is at this time not clear whether the parameter values chosen by Won and Friesner for their multi-parameter model are consistent with the thermal broadening and Stokes shift data for P-960. Within our model, ultra-fast decay of the primary electron donor state need not be invoked to account for the data, since (within the Born-Oppenheimer approximation) the primary electron donor state's significant charge-transfer character leads directly to strong linear electron-phonon coupling which renders the sharp zero-phonon holes very weak. We are not aware of any optical spectra for charge-transfer states of π-molecular systems that do not clearly indicate strong electron-phonon coupling. In our model the primary electron donor state is dirty in the sense that the absorption profile is determined by transitions to a wide distribution of mixed exciton-phonon levels. The primary electron donor state possesses significant charge-transfer character which leads to a large permanent dipole and its associated strong linear electron-phonon coupling. We note that Warshel and Parson [39] conclude that charge-transfer character can arise from mixing of the neutral excitonic and charge-transfer states of the special pair itself.

Concluding remarks

A theory for spectral hole burning has been developed that is valid for arbitrarily strong linear electron-phonon coupling and large site inhomogeneous line broadening. The Condon approximation is employed for the phonons which is known to be accurate for strongly allowed optical transitions, such as those of the photosynthetic pigments. The model calculations show that detailed studies of the hole profile dependence on the burn frequency (ω_B) can determine the site inhomogeneous line broadening (Γ_{inh}), the center of gravity of the zero-phonon site excitation energy distribution function relative to the absorption maximum, the Huang-Rhys factor (S) and effective phonon frequency (ω_m). For the case of strong linear coupling, the connection between the hole burning and thermal broadening data for the absorbing state has been given.

The theory successfully accounts for the gross and many of the fine features of the hole spectra for the primary electron donor states P-870, P-960 and P-700. The unifying picture which emerges is that the primary electron donor states are characterized by strong linear coupling ($S \gtrsim 4$) and large Γ_{inh}. It had been suggested earlier [9] that the strong coupling means that the primary electron donor states possess a significant charge-transfer character. Such character is supported by very recent Stark measurements [41]. The hole-burning data suggests that P-700, like P-870 and P-960, is a special pair. The large Γ_{inh} contribution to a primary electron donor state absorption profile

reflects the distribution of zero-phonon transition frequencies associated with an ensemble of spatially separated reaction center. Thus, there is no direct connection between Γ_{inh} and an average value for the energetic inequivalence (δE) between the Q_y states of the two monomers of a special pair. Nevertheless, it is known that protein interactions render the two monomers inequivalent [45]. The value of Γ_{inh} serves as an indicator for the magnitude of δE. For the interpretation of data which speak to excitonic resonance effects within the special pair, a consideration of the magnitudes of δE, the excitonic resonance matrix element and the homogeneous linewidth of the Q_y state is necessary.

The results presented here, together with the hole burning data for C-670 [14] and those from temperature-dependent time domain studies on the primary and secondary [15] electron-transfer processes of the reaction center of *Rb. sphaeroides* should be viewed as a whole. In doing so it becomes apparent that the linear electron-phonon coupling may play an important role in the early time events of photosynthesis. These include population of the primary electron donor state by excitation transport from the antenna or by direct optical excitation, and the primary electron-transfer from the primary electron donor state. Detailed quantum-mechanical transport theories which take into account strong linear coupling will need to address also the question of the distributions of pigment-state energies due to protein inhomogeneity. It is interesting to note that a large distribution width for the energy gap associated with a donor $\rightsquigarrow$ acceptor transport process is effectively compensated for by a large Huang-Rhys factor. An example of such a process would be the final trapping step in excitation transport from the antenna to primary electron donor state.

Finally, it appears that spectral hole burning is a powerful and generally applicable technique for probing the excited state structure and dynamics of photosynthetic systems. Very recently, hole burning and fluorescence line narrowing have been successfully applied by Avarmaa and Jaaniso [46] to the antenna chlorophyll of etiolated leaves. There would appear to be no reason why hole burning cannot be applied to a variety of pigment-protein complexes which have not been studied, e.g., PS II of green plants. In view of the recent calculations of Scherer and Fischer [47,48] and Warshel and Parson [49] on the electronic structure and electron-transfer dynamics of the reaction center of *Rps. viridis* it would also appear to be profitable to perform more extensive hole-burning experiments in the region of the P-960 absorption (also P-870). These calculations indicate that absorbing charge-separated states involving the special pair, the BChl monomer and bacteriopheophytin may be located in the near energetic vicinity of the primary electron donor state.

Acknowledgements

Ames Laboratory is operated for the U.S. Department of Energy by Iowa State University under Contract No. W-7405-ENG-82. This research was supported by the Director for Energy Research, Office of Basic Energy Science. We are indebted to D. Tiede of the Argonne National Laboratory for the reaction center samples of *Rps. viridis* and *Rb. sphaeroides* and to D. Holten and C. Kirmaier at Washington University for sending us their thermal broadening data on P-870 and P-960.

References

1 Kharlamov, B.M., Personov, R.I. and Bykovskaya, L.A. (1974) Opt. Commun. 12, 191–193.
2 Kharlamov, B.M., Personov, R.I. and Bykovskaya, L.A. (1975) Opt. Spectrosc. 39, 137–141.
3 Gorokhovskii, A.A., Karli, R.K. and Rebane, L.A. (1974) JETP Lett. 20, 216–218.
4 Small, G.J. (1983) in Spectroscopy and Excitation Dynamics of Condensed Molecular Systems of Series Modern Problems in Condensed Matter Sciences (Agranovich, V.M. and Hochstrasser, R.M., eds.), pp. 515–554, Elsevier/North-Holland, Amsterdam.
5 Friedrich, J. and Haarer, H. (1986) in Optical Spectroscopy of Glasses (I. Zschokke, ed.) pp. 149–198, D. Reidel, Dordrecht.
6 Rebane, L.A., Gorokhovskii, A.A. and Kikas, J.V. (1982) Appl. Phys. B29, 235–250.
7 Hayes, J.M., Jankowiak, R. and Small, G.J. (1988) in Topics in Current Physics, Vol. 44, Ch. 5, Persistent Spectral Hole-Burning: Science and Applications (Moerner, W.E., ed.), Springer-Verlag, Berlin.
8 Maslov, V.G., Chunaev, A.S. and Tugarinov, V.V. (1981) Mol. Biol. 15, 788–797.

9 Gillie, J.K., Fearey, B.L., Hayes, J.M., Small, G.J. and Golbeck, J.H. (1987) Chem. Phys. Lett. 134, 316–322.
10 Boxer, S.G., Lockhart, D.J. and Middendorf, T.R. (1986) Chem. Phys. Lett. 123, 476–482.
11 Meech, S.R., Hoff, A.J. and Wiersma, D.A. (1985) Chem. Phys. Lett. 121, 287–292.
12 Boxer, S.G., Middendorf, T.R. and Lockhart, D.J. (1986) FEBS Lett. 200, 237–241.
13 Meech, S.R., Hoff, A.J. and Wiersma, D.A. (1986) Proc. Natl. Acad. Sci. USA 83, 9464–9468.
14 Gillie, J.K., Hayes, J.M., Small, G.J. and Golbeck, J.H. (1987) J. Phys. Chem. 91, 5524–5527.
15 Bixon, M. and Jortner, J. (1986) J. Phys. Chem. 90, 3795–3800.
16 Parson, W.W., Woodbury, N.W.T., Becker, M., Kirmaier, C. and Holten, D. (1985) in Antennas and Reaction Centers of Photosynthetic Bacteria (Michel-Beyerle, M.E., ed.), pp. 278–285, Springer-Verlag, Berlin.
17 Hayes, J.M. and Small, G.J. (1986) J. Phys. Chem. 90, 4928–4931.
18 Scherer, P.O.J., Fischer, S.F., Hörber, J.K.H. and Michel-Beyerle, M.E. (1985) in Antennas and Reaction Centers of Photosynthetic Bacteria (Michel-Beyerle, M.E., ed.), pp. 131–137, Springer-Verlag, Berlin.
19 Pryce, M.H.L. (1965) in Phonons in Perfect Lattices and Lattices with Point Defects (Stevenson, R.W.H., ed.), pp. 403–448, Oliver and Boyd, London.
20 Rebane, K.K. (1970) Impurity Spectra of Solids, Plenum Press, New York.
21 Personov, R.I. (1983) in Spectroscopy and Excitation Dynamics of Condensed Molecular Systems (Agranovich, V.M. and Hochstrasser, R.M., ed.), pp. 555–620, Elsevier/North-Holland, Amsterdam.
22 Huang, K. and Rhys, A. (1951) Proc. Roy. Soc. A208, 352–365.
23 Kikas, J. (1978) Chem. Phys. Lett. 57, 511–513.
24 Kharlamov, B.M., Bykovskaya, L.A. and Personov, R.I. (1977) Chem. Phys. Lett. 50, 407–411.
25 Hayes, J.M., Fearey, B.L., Carter, T.P. and Small, G.J. (1986) Int. Rev. Phys. Chem. 5, 175–184.
26 Carter, T.P. and Small, G.J. (1985) Chem. Phys. Lett. 120, 178–182.
27 Woodbury, N.W.T. and Parson, W.W. (1984) Biochim. Biophys. Acta 767, 345–361.
28 Deisenhofer, J., Epp, O., Miki, K., Huber, R. and Michel, H. (1985) Nature 318, 618–624.
29 Knapp, E.W., Scherer, P.O.J. and Fischer, S.F. (1986) Biochim. Biophys. Acta 852, 295–305.
30 Chang, C.-H., Tiede, D., Tang, J., Smith, U., Norris, J. and Schiffer, M. (1986) FEBS Lett. 205, 82–86.
31 Sétif, P., Mathis, P. and Vänngård, T. (1972) Biochim. Biophys. Acta 767, 404–414.
32 Schaffernicht, H. and Junge, W. (1981) Photochem. Photobiol. 34, 223–232.
33 Ikegami, I. and Itoh, S. (1986) Biochim. Biophys. Acta 851, 75–85.
34 Martin, J.L., Breton, J., Hoff, A.J. and Antonetti, A. (1986) Proc. Natl. Acad. Sci. USA 83, 957–961.
35 Wasielewski, M.R. and Tiede, D.M. (1986) FEBS Lett. 204, 368–372.
36 Fenton, S.M., Pellin, M.J., Govindjee and Kaufman, K.J. (1976) FEBS Lett. 100, 1–4.
37 Owens, T.G., Webb, S.P., Mets, L., Alberts, R.S. and Fleming, G.R. (1987) Proc. Natl. Acad. Sci. USA 84, 1532–1536.
38 Brillante, A. and Philpott, M.R. (1980) J. Chem. Phys. 72, 4019–4030.
39 Parson, W.W., Sherz, A. and Warshel, A. (1985) in Antennas and Reaction Centers of Photosynthetic Bacteria (Michel-Beyerle, M.E., ed.), pp. 122–130, Springer-Verlag, Berlin.
40 Warshel, A. and Parson, W.W. (1987) J. Am. Chem. Soc. 109, 6143–6152.
41 Lockhart, D.J. and Boxer, S.G. (1987) Biochemistry 26, 664–668.
42 Scherer, P.O.J. and Fischer, S.F. (1986) Chem. Phys. Lett. 131, 153–159.
43 Rutherford, A.W. and Heathcote, P. (1985) Photosynth. Res. 6, 295–316.
44 Won, Y. and Friesner, R.A. (1987) Proc. Natl. Acad. Sci. USA 84, 5511–5515.
45 Tiede, D.M. (1987) Biochemistry 26, 397–410.
46 Avarmaa, R.A. and Jaaniso, R.H. (1987) Proceedings of Modern Methods of Laser Spectroscopy of Molecules on Low-Temperature Media, Tallinn, USSR.
47 Fischer, S.F. and Scherer, P.O.J. (1987) Chem. Phys. 115, 151–158.
48 Scherer, P.O.J. and Fischer, S.F. (1987) Chem. Phys. Lett. 141, 179–185.
49 Warshel, A. and Parson, W.W. (1988) J. Phys. Chem., in press.